Can the Low-Resolution Structures of Photointermediates of Bacteriorhodopsin Explain Their Crystal Structures?

Hironari Kamikubo and Mikio Kataoka
Graduate School of Materials Science, Nara Institute of Science and Technology, Ikoma, Nara 630-0192, Japan

ABSTRACT To understand the molecular mechanism of light-driven proton pumps, the structures of the photointermediates of bacteriorhodopsin have been intensively investigated. Low-resolution diffraction techniques have demonstrated substantial conformational changes at the helix level in the M and N intermediates, between which there are noticeable differences. The intermediate structures at atomic resolution have also been solved by x-ray crystallography. Although the crystal structures have demonstrated local structural changes, such as hydrogen bond network rearrangements including water molecules, the large conformational changes at the helix level are not necessarily observed. Furthermore, the two reported crystal structures of an intermediate accumulated using a common method were distinct. To reconcile these apparent discrepancies, low-resolution projection maps were calculated from the crystal structures and compared to the low-resolution intermediate structures obtained using native membranes. The crystal structures can be categorized into three groups, which qualitatively correspond to the low-resolution structures of the M1-type, M2-type, and N-type determined in the native membrane. Based on these results, we conclude that at least three types of intermediate structures play a role during the photocycle.

INTRODUCTION

Bacteriorhodopsin (bR) is a light-driven proton pump that uses absorbed photon energy to transport protons from the cytoplasm to the extracellular medium. bR is composed of seven transmembrane α-helices, which are named A–G, and short interconnecting loops. Upon absorption of light, bR undergoes the photoreaction cycle, during which there are several spectrally distinguishable mesostable photointermediates named the J, K, L, M, N, and O intermediates (Lanyi and Váró, 1995). Directional proton transport across a membrane is accomplished by several local proton transfers within the proton channel (Lanyi, 1993; Maeda, 1995). To understand the relationships among the local proton transfer reactions and the intermediates, the structures of the intermediates have been intensively investigated using various techniques.

The essential local proton transfers occur at the formation of the M and N intermediates. The structures of the M and N intermediates have been investigated by low-resolution diffraction methods under stabilizing conditions (Dencher et al., 1989; Kamikubo et al., 1996, 1997; Kataoka and Kamikubo, 2000; Koch et al., 1991; Nakasako et al., 1991) and by high-resolution electron diffraction and microscopy (Subramaniam et al., 1993; Vonck, 1996, 2000). The data demonstrated that the structures of the intermediates differed largely from the structure in the unphotolyzed state, where the major structural changes are seen around helices B, F, and G. We also found subtle but noticeable differences between the structures of the M and N intermediates and called these the M-type and N-type structures (Kamikubo et al., 1996, 1997; Kataoka and Kamikubo, 2000; Fig. 1).

Recently, based on the successful crystallization of bR (Luecke et al., 1998), x-ray crystallography has been intensively applied to the photointermediates in the latter half of the photocycle, the M and N intermediates (Facciotti et al., 2001; Lanyi and Schobert, 2002; Luecke et al., 1999, 2000a; Sass et al., 2000; Schobert et al., 2003; Takeda et al., 2004). The crystal structures of these intermediates demonstrated the role of internal water molecules and local structural changes such as the rearrangements of hydrogen bond networks near the chromophore. However, the large movement at the helix level demonstrated by the low-resolution diffraction techniques is not necessarily observed. Although the magnitude of the helix shift projected onto the membrane plane is almost 2 Å in the native membrane (Oka et al., 1999), the magnitude of the helix shift was in the range from 0 Å to 1 Å. Furthermore, the reported structural changes are somewhat different among the studies. For example, two crystal structures of the M intermediate of wild-type bR were independently reported by different groups. However, the reported structures are quite different (Sass et al., 2000; Schobert et al., 2003) although the same method was used in both studies to accumulate the intermediate. In crystallographic studies, it was proposed that the observed intermediates could be identified by the retinal configuration and the displacement of the water molecules and amino acid residues around the chromophore (Lanyi and Schobert, 2004; Schobert et al., 2003). By these criteria, one intermediate resembles the M1 state (Schobert et al., 2003), and the other resembles a later M state (M2 and/or MN; Sass et al., 2000). These discrepancies have led to

Submitted June 28, 2004, and accepted for publication November 24, 2004.

Address reprint requests to Dr. Mikio Kataoka, Graduate School of Materials Science, Nara Institute of Science and Technology (NAIST) Ikoma, Nara 630-0192 Japan. Tel.: 81-743-72-6100; Fax: 81-743-72-6109; E-mail: kataoka@ms.naist.jp.

0006-3495/05/03/1925/07 $2.00

doi: 10.1529/biophysj.104.045831

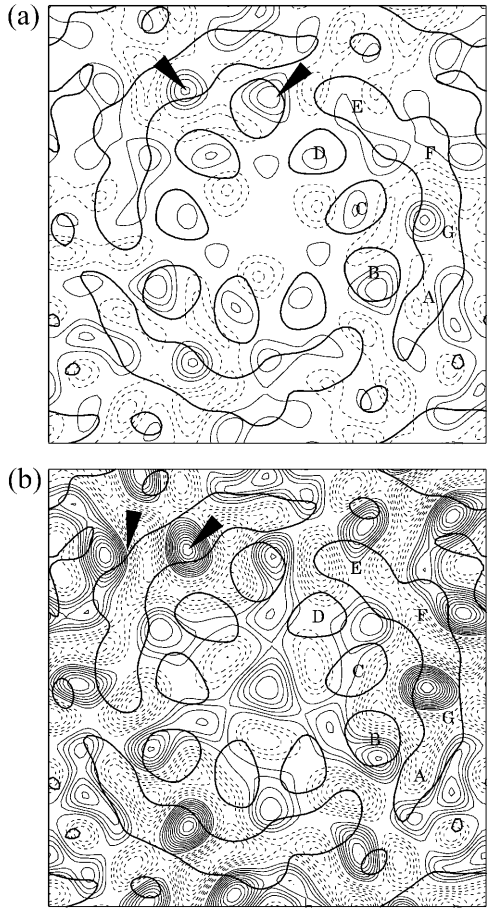

FIGURE 1 Electron difference maps of the M intermediate (*a*) and the N intermediate (*b*) obtained by low-resolution x-ray diffraction studies (Kamikubo et al., 1996; Nakasako et al., 1991), where the original intensity profiles were rescaled to compare with the calculated density maps obtained from the crystals. The increment is set to 500 for all maps, a solid line indicates positive density change, and a dashed line indicates negative density change. The arrows indicate the characteristic density changes for the intermediates.

misinterpretation of the role of the structural changes. Therefore, before interpreting the structural model, it is necessary to clarify which intermediate was used for the x-ray crystallographic experiments.

In some of the crystallographic studies, the observed intermediate was confirmed spectroscopically; however, performing spectroscopic measurements of a single crystal used in x-ray crystallography is technically difficult due to the small size and high optical density of the crystal. To overcome the difficulty of assignment of the intermediate during the diffraction experiment and reconcile the apparent discrepancies of the reported crystal structures, we now propose that the high-resolution crystal structures are connected to the structural changes observed in a native membrane. For this purpose, we calculated the low-resolution structure from each crystal structure and compared it to the previously observed low-resolution structures (Kamikubo et al., 1996; Nakasako et al., 1991). We found that the reported crystal structures of the intermediates can be classified into three groups and that each can be connected with a low-resolution structure. The differences among the crystal structures can be explained as differences in the structural states, such as M1-type, M2-type, and N-type. The good agreement between the crystallographic studies and the low-resolution diffraction studies confirms the existence of conformational substates during the latter half of the photocycle. The low-resolution diffraction technique has turned out to be a useful method for the evaluation of the intermediate state and has enabled the accurate interpretation of the intermediate structures.

MATERIALS AND METHODS

Calculation of low-resolution maps from crystal structures

Nine structural models of the M and N intermediate states and their related states were available in the protein database (Facciotti et al., 2001; Lanyi and Schobert, 2002; Luecke et al., 1999, 2000a; Sass et al., 2000; Schobert et al., 2003; Subramaniam and Henderson, 2000; Takeda et al., 2004). The Protein Data Bank codes for the structures of the intermediate state and the dark state are listed in Table 1. In this work, to compare the high-resolution and low-resolution structural changes (Kamikubo et al., 1996, 1997; Nakasako et al., 1991) during intermediate formation, the low-resolution difference density maps of the intermediate and the dark state were calculated using the reported crystal structures.

The models, except for 1FBB and 1FBK (determined by electron microscopy), were generated by x-ray crystallographic techniques using three-dimensional crystals that had different crystal systems ($P6_3$ or P622) relative to the system of the protein in native membrane (p3) used in the low-resolution x-ray diffraction and the electron diffraction studies. The tilt angle of the molecule to the crystal axis was slightly different between the three-dimensional crystal and the native membrane. For the sake of direct comparison, the structural model of the dark state of the three-dimensional crystal was rotated to fit the structural model of the native membrane (2BRD; Grigorieff et al., 1996). The conserved regions located in the transmembrane segments in both 2BRD and the x-ray crystallographic structure were selected for the fitting. These segments include Cα 9 $\sim$ 31 in helix A, 38 $\sim$ 62 in helix B, 80 $\sim$ 100 in helix C, 105 $\sim$ 127 in helix D, 134 $\sim$ 155 in helix E, 166 $\sim$ 191 in helix F, and 203 $\sim$ 226 in helix G. The obtained rotation matrix for the dark state model was also applied to the corresponding illuminated state model. The structural models of 1FBB and 1FBK obtained from native membrane were well superimposed on the template model (2BRD) without the fitting procedure and are used in the calculation below. The structure factors, $F(h,k,l)$, and the phases, $\delta(h,k,l)$, were calculated to 6 Å resolution based on a virtual crystal structure using the similar crystal system (P3) to that in a native membrane (p3). Only the atom coordinates listed in both the dark state and intermediate state were used in this calculation to extract density changes due to position changes. LSQKAB and SFTOOLS, parts of the Collaborative Computational Project, Number 4 (CCP4) program package, were used for the molecular rotation and structure factor calculation, respectively (CCP4, 1994). The low-resolution difference density maps projected onto the membrane surface were calculated by Eq. 1,

$$\Delta ED(x,y) \sim \sum_{(h,k)} \{F_{int}(h,k,0) - F_{dark}(h,k,0)\} \times \exp\{-2\pi i \times (hx+ky) + \delta_{dark}(h,k,0)\}, \quad (1)$$

where ΔED is the difference electron density, F_{int} and F_{dark} are structural factors for the intermediate state and the dark state, and $\delta_{dark}(h,k,0)$ is the

TABLE 1

Author	Specie	ID (dark)	ID (light)	Intermediate Reported	R-factor	Intermediate Assigned
Luecke et al. (1999)	D96N	1C8R	1C8S	M2′ (MN)	ND	-
Subramaniam et al. (2000)	D96G/F171C/F219L	1FBB	1FBK	Open-state	0.13	N-type
Sass et al. (2000)	Wild-type	1CWQ	1CWQ	M2	0.12	N-type (MN)
Schobert et al. (2003)	V49A	1P8U	1P8U	N′	0.05	M2-like
Facciotti et al. (2001)	Wild-type	1KG9	1KG8	Early-M	0.05	M2
Luecke et al. (2000a)	E204Q	1F50	1F4Z	M2	0.05	Prerelease M2
Takeda et al. (2004)	Wild-type	1QM8	1DZE	M	0.03	M1
Schobert et al. (2003)	Wild-type	1P8H	1P8H	M1	0.02	M1
Lanyi et al. (2002)	Wild-type	1M0M	1M0M	M1	0.01	M1

phase for the dark state. Equation 1 has also been applied to our low-resolution analysis.

RESULTS AND DISCUSSION

The available atomic coordinates of the intermediates present during the latter half of the photocycle and the dark state of bR are summarized in Table 1. The identity of each intermediate was originally designated by each investigator. Among the data set, the intermediate structure (1C8S) solved by Luecke et al. (1999) does not contain the cytoplasmic end of helices F and G because of disorder, making it impossible to extract the position change during intermediate formation. To characterize the reported intermediate crystal structures solved under the various conditions, low-resolution difference electron density maps were calculated from the atomic coordinates of the structures, except for 1C8S. The calculated low-resolution difference maps are shown in Fig. 2. The degree of calculated diffraction intensity changes is estimated as the R-factor, $\Sigma|dI(h,k)|/\Sigma I(h,k)$, the value of which is listed in Table 1. The values are widely distributed from 0.01 to 0.1. The calculated difference electron density maps in Fig. 2 are arranged in order of the R-factor value from *A* to *H*. The increment is 500 for all of the maps. The figures show that the magnitude of the density changes decreases with decreasing values of the R-factor.

According to the R-factor values and overall density changes, the difference projection maps can be classified into three groups: maps (Fig. 2, *a* and *b*) with large electron density changes (R-factor, 0.12 $\sim$ 0.13; Sass et al., 2000; Subramaniam and Henderson, 2000); maps (Fig. 2, *c–e*) with smaller electron density changes (R-factor, $\sim$ 0.05; Facciotti et al., 2001; Luecke et al., 2000a; Schobert et al., 2003); and maps (Fig. 2, *f–h*) without meaningful electron density changes (R-factor, 0.01 $\sim$ 0.03; Lanyi and Schobert, 2002; Schobert et al., 2003; Takeda et al., 2004). In the case of the low-resolution studies reported to date, the R-factor is $>$0.1 for N-type structures and $\sim$0.06 for M-type structures, which are comparable to the first two groups above.

We can compare these projection maps to the difference projection maps obtained using low-resolution diffraction techniques (Kamikubo et al., 1996, 1997; Kataoka and Kamikubo, 2000; Nakasako et al., 1991). As a reference to the M-type and N-type structural changes, the difference maps of the M intermediate (Nakasako et al., 1991) and the N intermediate (Kamikubo et al., 1996) are shown in Fig. 1, *a* and *b*, respectively. Larger density changes exist in the N intermediate (Fig. 1 *b*) than in the M intermediate (Fig. 1 *a*). As has been previously reported, there are also noticeable differences between the two structures (Kamikubo et al., 1996, 1997). In the M intermediate, characteristic density changes are observed around helices B and G; on the other hand, in the N intermediate such changes are observed around helices F and G (*arrows* in the figure). It should be noted that the prominent positive and negative density changes in helix F were assigned as the tilt of the cytoplasmic half of helix F by electron diffraction and microscopy (Subramaniam et al., 1993).

The maps with large density changes (Fig. 2, *a* and *b*) are comparable to the difference map of the N-type structure (Fig. 1 *b*). In particular, the changes in helix F, accompanied by characteristic positive and negative density changes, and the positive density change in helix G are obvious and are pointed out by arrows in the figure. From these data, we conclude that the structures of D96G/F171C/F219L (Subramaniam and Henderson, 2000) and photolyzed wild-type bR (Sass et al., 2000) solved in the crystal state reflect the N-type structure observed in the native membrane.

The difference projection map obtained from the M intermediate of wild-type bR trapped at 230 K reported by Facciotti et al. (2001) (Fig. 2 *d*) shows small but distinct positive density changes around helices G and B (*arrows* in the figure). These are characteristic features of the M-type structure (Fig. 1 *a*), suggesting that this intermediate state can be classified as an M intermediate with an M-type structure (Kamikubo et al., 1997; Nakasako et al., 1991) called M2. With a comparable R-factor to that of Facciotti's model, the difference map of Luecke et al. (2000a) (Fig. 2 *e*) shows slightly different features from that of Facciotti et al. (Fig. 2 *d*). Although the density changes around helices B and G are conserved, the positive density change in helix G seems to be smaller. Moreover, additive density changes are found around helices E and F (*white arrow* in the figure). Glu204 was proposed to be a candidate residue to release the proton to the extracellular medium after the proton was transferred from the Schiff base to Asp-85 during M

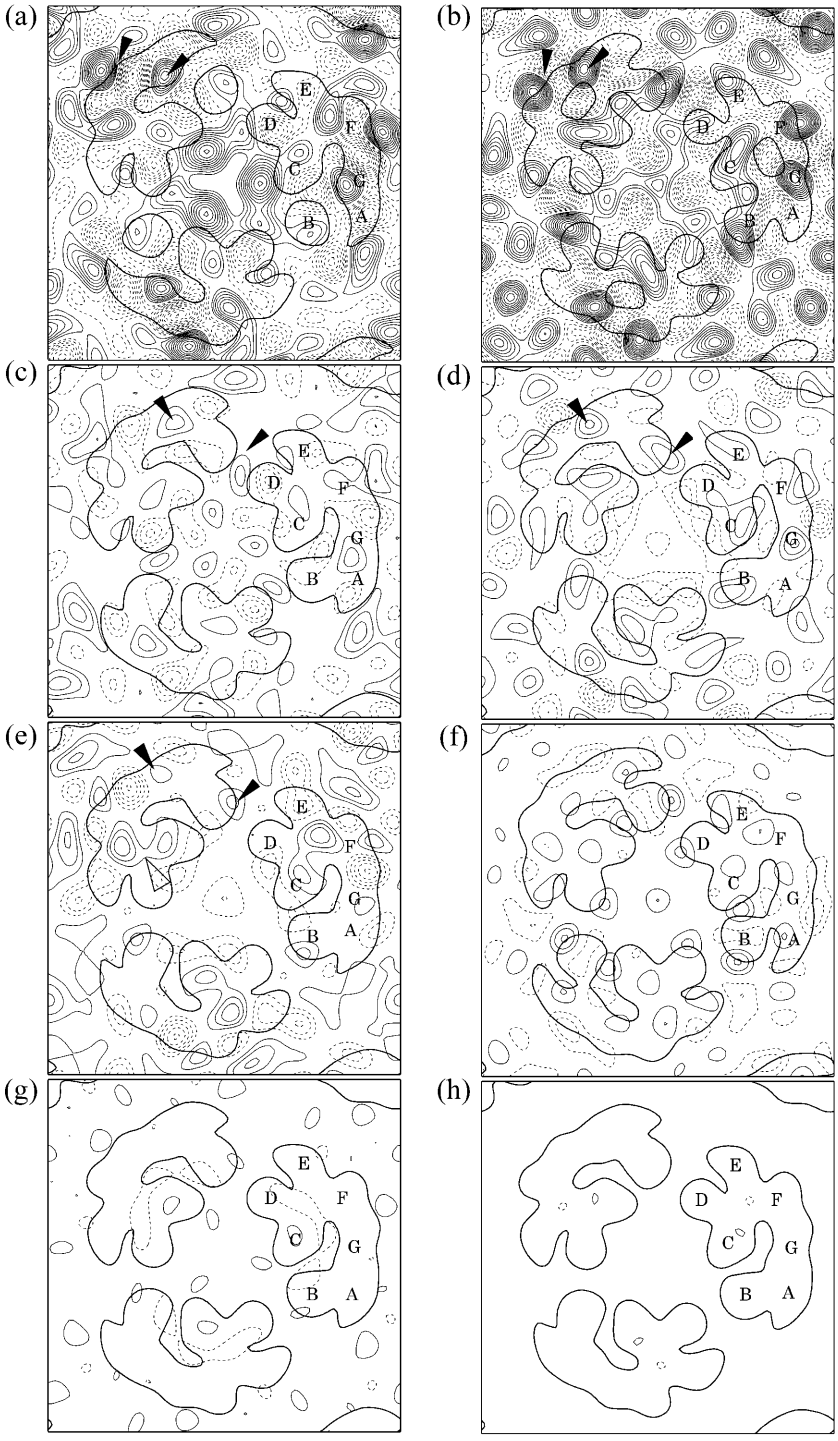

FIGURE 2 Electron difference maps of the intermediate and dark states calculated from reported crystallographic structures. (*a*) 1FBK − 1FBB (Subramaniam and Henderson, 2000), (*b*) $1CWQ_{light}$ − $1CWQ_{dark}$ (Sass et al., 2000), (*c*) $1P8U_{light}$ − $1P8U_{dark}$ (Schobert et al., 2003), (*d*) 1KG8 − 1KG9 (Facciotti et al., 2001), (*e*) 1F4Z − 1F50 (Luecke et al., 2000a), (*f*) 1DZE − 1QM8 (Takeda et al., 2004), (*g*) $1P8H_{light}$ − $1P8H_{dark}$ (Schobert et al., 2003), and (*h*) $1M0M_{light}$ − $1M0M_{dark}$ (Lanyi and Schobert, 2002), referring to Table 1. In calculation of density changes, the scattering factors were normalized, and the density change values can be compared with each other. The increment is set to 500 for all maps, a solid line indicates positive density change, and a dashed line indicates negative density change. The solid arrows indicate the characteristic density changes in the difference maps which are referred in the assignment of the structural state. The open arrow in (*e*) shows the novel density change in the E204Q mutant.

intermediate formation. The replacement of Glu204 with Gln decreased the proton release activity, suggesting that the accumulated mutant M intermediate is a precursor of the normal postrelease M2 intermediate (Brown et al., 1995). The novel part of the structural changes of E204Q might be related to the blocked release of a proton to the extracellular medium.

Although the accumulated V49A mutant intermediate was assigned to the N-like intermediate, called the N′ intermediate, the R-factor of the V49A structure is similar to that of the M-type. Indeed, the map of V49A (Fig. 2 *c*) shows characteristic features of the M-type structure rather than the features of the N-type. The overall density changes are comparable to those in the structure of Facciotti et al. (Fig. 2 *d*),

where characteristic positive density changes around helices B and G can be seen (*arrows* in the figure), and the density change around helix F is smaller than observed in the N-type. Schobert et al. (2003) also noted the discrepancy between the N′ intermediate structure and the N-type structure. In the N′ intermediate, the tilt of helix F results in a cavity between Asp-96 and cytoplasm that is too small to accommodate water molecules; this is consistent with the smaller density change observed around helix F in the map of V49A (Fig. 2 *c*). It was reported that the prolonged N′ intermediate generated using the V49A mutant under acidic conditions is a post-N intermediate that forms after reprotonation of Asp-96 from cytoplasm during the N intermediate decay process (Schobert et al., 2003). To reprotonate Asp-96 during N′ formation, the environment around Asp-96 should become hydrophobic; in other words, the open channel observed in the N intermediate should close. It is plausible that the M-like difference map reflects a transient structure that exists when the N-type structure returns to the initial structure.

The rest of the maps (Fig. 2, *f–h*) show almost no density change. Sass et al. (1997) reported no density changes in the M intermediate under highly anhydrous conditions; this is the so-called M1 state. The projection maps showing almost no density changes probably reflect the M1 state. To discriminate between the M1 state, which lacks meaningful density changes, and the M2 state with the M-type structure, we will refer to these states as M1-type and M2-type, respectively.

Some contradictions do remain in the attribution of the intermediates. Sass et al. (2000) and Facciotti et al. (2001) assigned their accumulated intermediates as M2 and early-M, respectively. In contrast, this work suggests that these observed structural states are N-type for Sass et al. (2000) and M2-type for Facciotti et al. (2001).

In the study by Sass et al. (2000), the intermediate was accumulated by illuminating a crystal of wild-type bR at 295 K for 1 s, followed by rapid cooling to 100 K. In this way, a mixture of intermediates and dark state bR was produced, where 60%–70% of the bR molecules were accumulated as the M intermediate, 30%–40% of the molecules were in the dark state, and a small amount of the N intermediate was present. Because the amplitude of structural changes in the N intermediate is quite a bit larger than that in the M intermediate, even a small amount of the N intermediate could affect the structural model; this is one reason for the noted discrepancy. Moreover, among the crystallographic studies, the contradiction in the assignment of the intermediate was pointed out (Schobert et al., 2003). Although Schobert et al. followed the method of Sass et al. to accumulate the M intermediate, the structure they observed was quite different from that of Sass et al. (see above). It was proposed that the observed intermediate could be assigned by the retinal configuration and the displacement of the water molecules and amino acid residues around the chromophore (Lanyi and Schobert, 2004; Schobert et al., 2003). By these criteria, the structure of Schobert et al. shows the characteristic features of M1, and the structure of Sass et al. shows the features of M2 and/or later M (Schobert et al., 2003). It is expected to accumulate the M2 and/or later M under the solution condition for the crystallization (pH 5.6; Zimanyi et al., 1992). However, the observed intermediate in the study of Schobert et al. was assigned as the M1 state. Schobert et al. pointed out the possibility that the actual pH in their crystal would be lower for proton release than the pKa, promoting the M1 and M2 equilibrium favors the earlier (Schobert et al., 2003). The reason for these discrepancies is unclear, but it is a fact that the accumulated intermediate is highly affected by unknown subtle perturbations in the conditions (actual pH in a crystal, temperature, light source, hydration level, etc.), indicating that it is necessary to designate the observed intermediate by criteria based on the observed crystal structure.

The early-M intermediate, assigned by Facciotti's study, is also apparently different from M2, the intermediate observed in this study (Fig. 2 *d*). However, their assignment of an early-M intermediate is slightly ambiguous. They assigned ''early''-M to the coupled state, and ''late''-M (MN) was accompanied by a large conformational change. Their early-M intermediate includes both the M1 and M2 intermediates in our notation. Actually, Facciotti et al. (2001) suggested that their intermediate structure shared similar features with the M2 intermediate of E204Q. By criteria based on the crystal structure, the structure of Facciotti et al. is also proposed to resemble that of the M2 state, in which the nitrogen atom of the Schiff base is oriented toward the cytoplasmic channel and the side chain of Arg 82 moves away from its original position. This study confirms that the intermediate state observed by Facciotti et al. corresponds to the M2 state of the early-M intermediates. On the other hand, the structural state (1M0M; Fig. 2 *h*) of Lanyi and Schobert is assigned to be the M1 state. The intermediate was accumulated by illumination of a crystal under low temperature, as is the similar method of Facciotti et al. (Lanyi and Schobert, 2002). However, the temperature of Facciotti's study (230 K) was slightly higher than that in Lanyi and Schobert (210 K). It was reported that the accumulated substate of the M state was affected by small temperature differences (Vonck et al., 1994). Thus the temperature to trap the photointermediate would be one of the reasons for the differences among the observed states.

We were able to categorize the reported intermediate crystal structures into three types of structural state (M1-type, M2-type, and N-type), as proposed by the previous low-resolution diffraction studies, without any serious contradictions. To compare the predicted crystal structures of the M2- and N-types, the global structural changes assigned to the M2-type structure (Facciotti et al., 2001) and the N-type structure (Sass et al., 2000) are shown in Fig. 3, *a* and *b*, respectively. For the M2-type structure, prominent changes are observed around helix G (Fig. 3 *a*). In the dark state, the

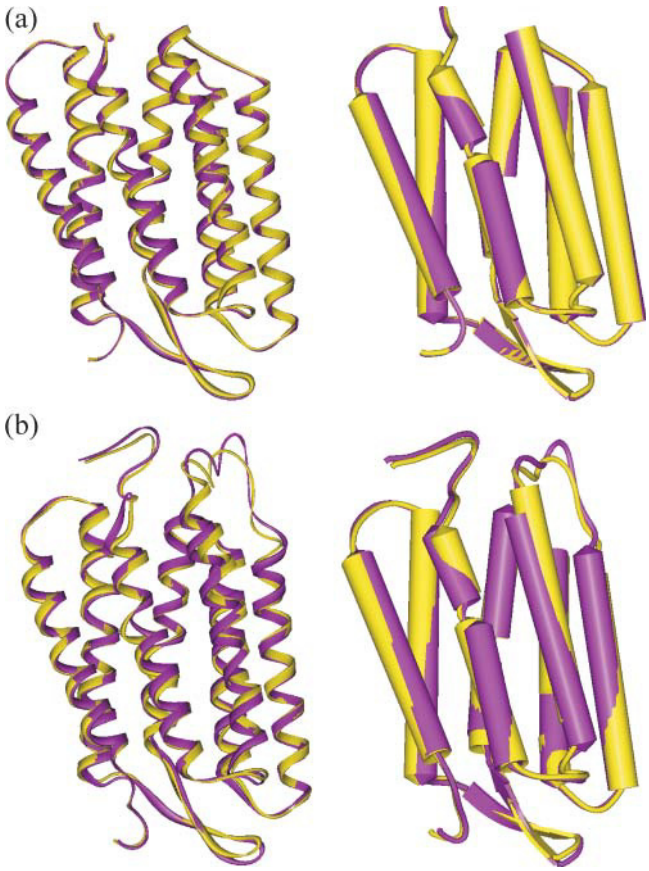

FIGURE 3 Schematic models (*yellow*) of the M2-type (*a*) and N-type (*b*) structures proposed by comparison of the low-resolution structures corresponding to 1KG8 by Facciotti et al. (2001) and 1CWQ by Sass et al. (2000). For the sake of comparison, the corresponding dark state model is represented in purple.

middle of helix G is kinked by a π-bulge around residue 215. Upon absorption of light, the kinked helix is relaxed into a normal helical conformation. It has been reported that two water molecules are affected by this structural relaxation and may participate in forming a hydrogen bond network between the Schiff base and D96 in the intermediate state (Luecke, 2000b). The N-type structure shows an additional change in the tilt of helix F when compared to the M-type structure (Fig. 3 *b*). According to the crystal structure of the N-type (1CWQ), a cavity connecting the protein surface and Asp-96 is found in the cytoplasmic channel, which is mediated by the tilt of helix F. At the N intermediate, to deprotonate Asp-96 during its formation and to arrange the following reprotonation of Asp-96 from cytoplasm during the decay process, the environment in the cytoplasmic channel should be hydrophilic, which is actually established by the N-type structure. This is exactly the movement expected from the low-resolution diffraction studies (Kamikubo et al., 1996; Subramaniam et al., 1993; Vonck, 1996) and electron paramagnetic resonance studies (Rink et al., 2000; Thorgeirsson et al., 1997) and corresponds to the opening of the cytoplasmic channel. We believe that the tilt of helix F shown in this structure reflects the real structural change occurring in the native membrane. The reported crystal structures were interpreted with the low-resolution structures. We were able to demonstrate that there are at least three different structural states, M1, M2, and N, in the photolyzed crystal structures.

Takeda et al. (2004) found the sliding motion of helix G. They claimed that the sliding motion is essential for the proton pump. Such a sliding motion, however, cannot be observed in the other crystal structures. Takeda et al. interpreted this discrepancy as the difference in crystalline space group. Since the low-resolution diffraction method gives only a two-dimensional projection map, the sliding motion, if any, cannot be distinguished with this method. Takeda et al., on the other hand, are not necessarily opposed to the role of the F helix tilt.

Based on the low-resolution diffraction studies, subtle but meaningful structural differences between the M and N intermediates have been described (Kamikubo et al., 1996; Kataoka and Kamikubo, 2000). It was also reported that these two structural states are in equilibrium depending on the membrane hydration level (Kamikubo et al., 1997), suggesting that the transition between the M2- and N-type structures is closely related to the ability of water molecules to access the cytoplasmic channel. Further, this transition is likely to participate in the regulation of deprotonation and reprotonation of Asp-96 during the latter half of the photocycle. A recent time-resolved x-ray diffraction study on native membrane demonstrated the existence of a structural transition from the M2-type to the N-type (Oka et al., 2000, 2002). On the other hand, the differences between the difference electron density maps of the M- and N-type structures are subtle. Furthermore, it cannot be determined whether the observed difference in the amplitude of the density change depends on intrinsic structural aspects of these intermediates or on the equilibrium between the two structural states. This led Subramaniam et al. (1999) and Sass et al. (1997) to suggest that the structural differences between the M and N states are trivial. To confirm the distinction between the M-type structures and the N-type structure, it has been necessary to resolve the high-resolution structural model for each state. Based on the fact that it is possible to categorize the reported crystal structures into three types of structural state, we conclude that the structures of M2 and N are substantially different and that the difference stressed by our group really occurs during the photocycle. We propose that high pump activity is accomplished by synchronization of chromophore structural changes with hydrogen bonding network rearrangements in the vicinity of the chromophore and tertiary protein structural changes under physiological conditions (Kataoka and Kamikubo, 2000). Our proposed conformation-controlled conformational change model (Kataoka and Kamikubo, 2000) has been confirmed and refined to a more elegant model based on analysis of the reported crystal structures (Lanyi and Schobert, 2003, 2004).

REFERENCES

Brown, L. S., J. Sasaki, H. Kandori, A. Maeda, R. Needleman, and J. K. Lanyi. 1995. Glutamic acid 204 is the terminal proton release group at the extracellular surface of bacteriorhodopsin. *J. Biol. Chem.* 270: 27122–27126.

Collaborative Computational Project, Number 4. 1994. The CCP4 Suite: programs for protein crystallography. *Acta. Crystallogr. Sect. D. Biol. Crystallogr.* 50:760–763.

Dencher, N. A., D. Dresselhaus, G. Zaccai, and G. Büldt. 1989. Structural changes in bacteriorhodopsin during proton translocation revealed by neutron diffraction. *Proc. Natl. Acad. Sci. USA.* 86:7876–7879.

Facciotti, M. T., S. Rouhani, F. T. Burkard, F. M. Betancourt, K. H. Downing, R. B. Rose, G. McDermott, and R. M. Glaeser. 2001. Structure of an early intermediate in the M-state phase of the bacteriorhodopsin photocycle. *Biophys. J.* 81:3442–3455.

Grigorieff, N., T. A. Ceska, K. H. Downing, J. M. Baldwin, and R. Henderson. 1996. Electron-crystallographic refinement of the structure of bacteriorhodopsin. *J. Mol. Biol.* 259:393–421.

Kamikubo, H., M. Kataoka, G. Varo, T. Oka, F. Tokunaga, R. Needleman, and J. K. Lanyi. 1996. Structure of the N intermediate of bacteriorhodopsin revealed by x-ray diffraction. *Proc. Natl. Acad. Sci. USA.* 93: 1386–1390.

Kamikubo, H., T. Oka, Y. Imamoto, F. Tokunaga, J. K. Lanyi, and M. Kataoka. 1997. The last phase of the reprotonation switch in bacteriorhodopsin: the transition between the M-type and the N-type protein conformation depends on hydration. *Biochemistry.* 36:12282–12287.

Kataoka, M., and H. Kamikubo. 2000. Structures of photointermediates and their implications for the proton pump mechanism. *Biochim. Biophys. Acta.* 1460:166–176.

Koch, M. H., N. A. Dencher, D. Oesterhelt, H. J. Plohn, G. Rapp, and G. Büldt. 1991. Time-resolved x-ray diffraction study of structural changes associated with the photocycle of bacteriorhodopsin. *EMBO J.* 10:521–526.

Lanyi, J. K. 1993. Proton translocation mechanism and energetics in the light-driven pump bacteriorhodopsin. *Biochim. Biophys. Acta.* 1183:241–261.

Lanyi, J. K., and B. Schobert. 2002. Crystallographic structure of the retinal and the protein after deprotonation of the Schiff base: the switch in the bacteriorhodopsin photocycle. *J. Mol. Biol.* 321:727–737.

Lanyi, J. K., and B. Schobert. 2003. Mechanism of proton transport in bacteriorhodopsin from crystallographic structures of the K, L, M1, M2, and M2′ intermediates of the photocycle. *J. Mol. Biol.* 328:439–450.

Lanyi, J. K., and B. Schobert. 2004. Local-global conformational coupling in a heptahelical membrane protein: transport mechanism from crystal structures of the nine states in the bacteriorhodopsin photocycle. *Biochemistry.* 43:3–8.

Lanyi, J. K., and G. Váró. 1995. The photocycle of bacteriorhodopsin. *Isr. J. Chem.* 35:365–386.

Luecke, H. 2000b. Atomic resolution structures of bacteriorhodopsin photocycle intermediates: the role of discrete water molecules in the function of this light-driven ion pump. *Biochim. Biophys. Acta.* 1460:133–156.

Luecke, H., H. T. Richter, and J. K. Lanyi. 1998. Proton transfer pathways in bacteriorhodopsin at 2.3 angstrom resolution. *Science.* 280:1934–1937.

Luecke, H., B. Schobert, J. P. Cartailler, H. T. Richter, A. Rosengarth, R. Needleman, and J. K. Lanyi. 2000a. Coupling photoisomerization of retinal to directional transport in bacteriorhodopsin. *J. Mol. Biol.* 300:1237–1255.

Luecke, H., B. Schobert, H. T. Richter, J. P. Cartailler, and J. K. Lanyi. 1999. Structural changes in bacteriorhodopsin during ion transport at 2 angstrom resolution. *Science.* 286:255–261.

Maeda, A. 1995. Application of FTIR spectroscopy to the structural study on the function of bacteriorhodopsin. *Isr. J. Chem.* 35:387–400.

Nakasako, M., M. Kataoka, Y. Amemiya, and F. Tokunaga. 1991. Crystallographic characterization by x-ray diffraction of the M-intermediate from the photo-cycle of bacteriorhodopsin at room temperature. *FEBS Lett.* 292:73–75.

Oka, T., H. Kamikubo, F. Tokunaga, J. K. Lanyi, R. Needleman, and M. Kataoka. 1999. Conformational change of helix G in the bacteriorhodopsin photocycle: investigation with heavy atom labeling and x-ray diffraction. *Biophys. J.* 76:1018–1023.

Oka, T., N. Yagi, T. Fujisawa, H. Kamikubo, F. Tokunaga, and M. Kataoka. 2000. Time-resolved x-ray diffraction reveals multiple conformations in the M-N transition of the bacteriorhodopsin photocycle. *Proc. Natl. Acad. Sci. USA.* 97:14278–14282.

Oka, T., N. Yagi, F. Tokunaga, and M. Kataoka. 2002. Time-resolved x-ray diffraction reveals movement of F helix of D96N bacteriorhodopsin during M-MN transition at neutral pH. *Biophys. J.* 82:2610–2616.

Rink, T., M. Pfeiffer, D. Oesterhelt, K. Gerwert, and H. J. Steinhoff. 2000. Unraveling photoexcited conformational changes of bacteriorhodopsin by time resolved electron paramagnetic resonance spectroscopy. *Biophys. J.* 78:1519–1530.

Sass, H. J., G. Büldt, R. Gessenich, D. Hehn, D. Neff, R. Schlesinger, J. Berendzen, and P. Ormos. 2000. Structural alterations for proton translocation in the M state of wild-type bacteriorhodopsin. *Nature.* 406:649–653.

Sass, H. J., R. Gessenich, M. H. Koch, D. Oesterhelt, N. A. Dencher, G. Büldt, and G. Rapp. 1997. The tertiary structural changes in bacteriorhodopsin occur between M states: x-ray diffraction and Fourier transform infrared spectroscopy. *EMBO J.* 16:1484–1491.

Schobert, B., L. S. Brown, and J. K. Lanyi. 2003. Crystallographic structures of the M and N intermediates of bacteriorhodopsin: assembly of a hydrogen-bonded chain of water molecules between Asp-96 and the retinal Schiff base. *J. Mol. Biol.* 330:553–570.

Subramaniam, S., M. Gerstein, D. Oesterhelt, and R. Henderson. 1993. Electron diffraction analysis of structural changes in the photocycle of bacteriorhodopsin. *EMBO J.* 12:1–8.

Subramaniam, S., and R. Henderson. 1999. Electron crystallography of bacteriorhodopsin with millisecond time resolution. *J. Struct. Biol.* 128: 19–25.

Subramaniam, S., and R. Henderson. 2000. Molecular mechanism of vectorial proton translocation by bacteriorhodopsin. *Nature.* 406:653–657.

Takeda, K., Y. Matsui, N. Kamiya, S. Adachi, H. Okumura, and T. Kouyama. 2004. Crystal structure of the M intermediate of bacteriorhodopsin: allosteric structural changes mediated by sliding movement of a transmembrane helix. *J. Mol. Biol.* 341:1023–1037.

Thorgeirsson, T. E., W. Xiao, L. S. Brown, R. Needleman, J. K. Lanyi, and Y. K. Shin. 1997. Transient channel-opening in bacteriorhodopsin: an EPR study. *J. Mol. Biol.* 273:951–957.

Vonck, J. 1996. A three-dimensional difference map of the N intermediate in the bacteriorhodopsin photocycle: part of the F helix tilts in the M to N transition. *Biochemistry.* 35:5870–5878.

Vonck, J. 2000. Structure of the bacteriorhodopsin mutant F219L N intermediate revealed by electron crystallography. *EMBO J.* 19:2152–2160.

Vonck, J., B. G. Han, F. Burkard, G. A. Perkins, and R. M. Glaeser. 1994. Two progressive substrates of the M-intermediate can be identified in glucose-embedded, wild-type bacteriorhodopsin. *Biophys. J.* 67:1173–1178.

Zimanyi, L., G. Váró, M. Chang, B. Ni, R. Needleman, and J. K. Lanyi. 1992. Pathways of proton release in the bacteriorhodopsin photocycle. *Biochemistry.* 31:8535–8543.